Paper 150

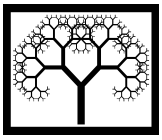

Proceedings of the Eleventh International Conference
on Computational Structures Technology,
B.H.V. Topping, (Editor),
Civil-Comp Press, Stirlingshire, Scotland

Three-Dimensional Cohesive Crack Propagation using Hybrid-Trefftz Finite Elements

G. Edwards, C.J. Pearce and Ł. Kaczmarczyk
Infrastructure & Environment Research Division
School of Engineering, University of Glasgow, United Kingdom

Abstract

A finite element formulation for the modelling of cohesive cracks in quasi-brittle materials is presented. This combines tetrahedral hybrid-Trefftz stress elements for the bulk material and continuous triangular interface elements for the discrete cracks which contain a softening law using fracture energy to capture the post-peak response. An algorithm is presented for an adaptive procedure which allows the interface element to be inserted when the tensile strength across an inter element boundary is exceeded. A simple three-dimensional numerical example is also presented to verify both the interface element formulation and the crack insertion algorithm.

Keywords: fracture, hybrid-Trefftz, interface, softening, crack-insertion, three-dimensional, heterogeneous.

1 Introduction

The mechanical behaviour of many materials is rooted in the behaviour of the heterogeneous microstructure and there are a number of microstructure-driven phenomena, such as wave dispersion and size effects, that can be investigated by a detailed modelling at the microstructure level. This paper is based on the work of Kaczmarczyk and Pearce [1], which developed a 2D hybrid-Trefftz stress element formulation for the modelling of cohesive cracks in heterogeneous materials subject to static loads and extends it into three dimensions.

Cracking can be modelled in a number of different ways but there are three main approaches[2], namely smeared crack models, lattice models and discrete crack models. Smeared crack models are attractive as the problem can be solved within a continuum setting whereby the deterioration process is captured via a stress-strain relationship, smearing the damage over the continuum. In lattice models, the continuum

is replaced by and equivalent lattice of beam elements which can have the microstructure mapped onto it and thus allow the mircostructure to influence the cracking results [2]. Finally, discrete crack models introduce displacement discontinuities into the formulation where the relationship is controlled by a traction-displacement jump relationship rather than a stress-strain relationship. The discrete crack model is the approach adopted in this paper. Here, continuous interface elements will be used where the elements are integrated over the relevant faces of the 10-noded tetrahedrons that are used to describe the 3D continuum. A linear softening law will be incorporated into the interface elements and a secant stiffness matrix will be used in the non-linear analysis. A disadvantage of using this method is that the crack path must be restricted to inter-element boundaries. However, this issue can be alleviated to a large extent by ensuring a random mesh is generated. It is also believed that the explicit modelling of heterogeneities will have a bigger influence on the crack path than the underlying mesh[1]. This paper focuses on the modelling of discrete cracks in 3D and the modelling of heterogeneities is an issue for future publications.

When using interface elements, two approaches can be adopted. Firstly, an interface element can be inserted between every face in the continuum *a priori* with a high initial stiffness before a softening law is introduced when a stress threshold is reached. Secondly, interface elements can be inserted when, or if, they are required. The work in this paper will implement the second option and an algorithm will be presented, using the work proposed in [3] as motivation.

Finally, a simple numerical example will be shown that incorporates both the crack insertion algorithm and the interface elements with relevant results being presented.

Voigt notation is adopted throughout the paper.

2 Hybrid-Trefftz Stress Formulation

Hybrid finite element formulations have advantages over classical finite element formulations in terms of their ability to estimate stresses [4]. This is of great importance when investigating fracture in a heterogeneous material, such as concrete, where an accurate representation of the stress state is a necessity. The limitation of the classical element is that it has one approximation over the element domain, usually for displacements, which is then related to the strains by a differential operator and the stresses by a constitutive relationship. However, in a hybrid element there are 2 fields present in a single element. One field is an approximation over the element domain, Ω_e, while the other is an approximation over the element boundary, Γ_e.

Hybrid stress elements, used in this paper, are elements that approximate stresses within the domain and displacements over the boundary. Trefftz elements, used in the formulation presented, use Trefftz functions to approximate the stresses in the element domain that *a priori* satisfy the linear momentum balance equation. In the context of this work, the major advantages of using the hybrid-Trefftz stress formulations for modelling cracking are as follows; in static analyses the formulation allows for

an sparse symmetric stiffness matrix to be obtained while integrating along element boundaries only, which enables the user to generate arbitrary elements which can be convex or concave in shape; the formulation allows for accurate representation of stress concentrations; and, unlike classical finite elements, inconsistencies between the stress field within the bulk elements and traction field in the cohesive element are avoided due to the higher approximation basis available.

2.1 Element Formulation

This section will outline the formulation of the hybrid-Trefftz stress element and is largely based on the work by Kaczmarczyk and Pearce [1] and Teixeira de Freitas [5]. The governing equations for a typical element, Ω_e, with a boundary, $\Gamma = \Gamma_\sigma \cup \Gamma_u$ where $\Gamma_\sigma \cap \Gamma_u = \oslash$ are as follows:

$$\mathbf{L}^{\mathbf{T}}\boldsymbol{\sigma} = 0 \quad \text{in}\,\Omega_e \tag{1}$$

$$\boldsymbol{\epsilon} = \mathbf{C}\boldsymbol{\sigma} \quad \text{in}\,\Omega_e \tag{2}$$

$$\mathbf{L}\mathbf{u} = \boldsymbol{\epsilon} \quad \text{in}\,\Omega_e \tag{3}$$

$$\mathbf{u} = \overline{\mathbf{u}} \quad \text{on}\,\Gamma_u \tag{4}$$

$$\mathbf{N}\boldsymbol{\sigma} = \bar{\mathbf{t}} \quad \text{on}\,\Gamma_\sigma \tag{5}$$

where $\mathbf{L}$ is a differential operator, $\mathbf{C}$ is the compliance matrix and $\mathbf{N}$ is the unit normal of the element boundary. Body forces have been ignored for simplicity. As mentioned previously, the stresses are approximated using approximation functions which *a priori* satisfy (1) as follows:

$$\boldsymbol{\sigma} = \mathbf{S}_\mathbf{v}\mathbf{v} \implies \mathbf{L}^{\mathbf{T}}\mathbf{S}_\mathbf{v} = 0 \tag{6}$$

where $\mathbf{S}_\mathbf{v}$ contains the approximation functions and $\mathbf{v}$ contains the generalised stress degrees of freedom. Using the relationship in (6), the tractions on the surface of an element are given by:

$$\mathbf{t} = \mathbf{N}\boldsymbol{\sigma} = \mathbf{N}\mathbf{S}_\mathbf{v}\mathbf{v} \tag{7}$$

The Trefftz functions in $\mathbf{S}_\mathbf{v}$must be designed so that they are not dependent on any particular constitutive law and can be arrived at in a number of ways, such as from the Airy's stress function. The functions are also element dependent which means that separate approximation bases can be used for different elements in a mesh.

The traction boundary condition is satisfied in a weighted residual sense:

$$\int_\Gamma \mathbf{w}_\mathbf{1}^T(\mathbf{N}\boldsymbol{\sigma} - \bar{\mathbf{t}})d\Gamma = 0 \implies \int_\Gamma \mathbf{w}_\mathbf{1}^T(\mathbf{N}\mathbf{S}_\mathbf{v}\mathbf{v})d\Gamma = \int_\Gamma \mathbf{w}_\mathbf{1}^T\bar{\mathbf{t}}d\Gamma \tag{8}$$

where $\mathbf{w_1}$ is an appropriate weighting function. The kinematic boundary condition is also enforced in a weighted residual sense:

$$\int_{\Omega} \mathbf{w_2}^T(\boldsymbol{\epsilon} - \mathbf{L}\mathbf{u})d\Omega = 0 \tag{9}$$

A weak form of this equation is determined via integration by parts using Green's theorem to give:

$$\int_{\Omega} \mathbf{w_2}^T \boldsymbol{\epsilon} d\Omega + \int_{\Omega} (\mathbf{L}\mathbf{w_2})^T \mathbf{u} d\Omega - \int_{\Gamma_\sigma} (\mathbf{N}\mathbf{w_2})^T \mathbf{u} d\Gamma = \int_{\Gamma_u} (\mathbf{N}\mathbf{w_2})^T \bar{\mathbf{u}} d\Gamma \tag{10}$$

where $\mathbf{w_2}$ is another appropriate weighting function ensuring that all integrals have the unit of work. In the above equation, the displacements have been split into two parts associated with the traction and kinematic boundary conditions. Looking at the most general case for $\Gamma = \Gamma_\sigma \cup \Gamma_u$ where $\Gamma_\sigma \cap \Gamma_u = \oslash$ an additional approximation basis is required on the boundary of the element to ensure that the independence of statics and kinematics is maintained[1]. This independent approximation is valid on Γ_σ and given by:

$$\mathbf{u_\Gamma} = \mathbf{U_\Gamma}\mathbf{q} \tag{11}$$

where $\mathbf{q}$ is the generalised displacement degrees of freedom and $\mathbf{U_\Gamma}$ contains the displacement approximation functions along the element boundary. The approximation functions used here are the isoparametric shape functions for a 6-noded triangle. Choosing weighting function such that all integrals have the unit of work, (8) and (10) become:

$$\int_{\Gamma} \mathbf{U}_\Gamma^T \mathbf{N}\mathbf{S}_\mathbf{v}\mathbf{v} d\Gamma = \int_{\Gamma_\sigma} \mathbf{U}_\Gamma^T \bar{\mathbf{t}} d\Gamma \tag{12}$$

$$\int_{\Omega} \mathbf{S}_\mathbf{v}^T \boldsymbol{\epsilon} d\Omega + \int_{\Omega} (\mathbf{L}\mathbf{S}_\mathbf{v})^T \mathbf{u} d\Omega - \int_{\Gamma_\sigma} \mathbf{U_\Gamma} (\mathbf{N}\mathbf{S}_\mathbf{v})^T \mathbf{q} d\Gamma = \int_{\Gamma_u} (\mathbf{N}\mathbf{S}_\mathbf{v})^T \bar{\mathbf{u}} d\Gamma \tag{13}$$

From (1) the second term in (13) can be eliminated and the remaining volume integral can be converted into a boundary integral only. The two equations presented are coupled and can be written in matrix format as follows:

$$\begin{bmatrix} \mathbf{F} & -\mathbf{A}^\mathbf{T} \\ -\mathbf{A} & 0 \end{bmatrix} \begin{bmatrix} \mathbf{v} \\ \mathbf{q} \end{bmatrix} = \begin{bmatrix} \mathbf{p_u} \\ -\mathbf{p_\sigma} \end{bmatrix} \tag{14}$$

where

$$\mathbf{F} = \int_{\mathbf{\Omega}} \mathbf{S}_\mathbf{v}^\mathbf{T} \mathbf{C} \mathbf{S}_\mathbf{v} \mathbf{d\Omega} = \int_{\mathbf{\Gamma}} \mathbf{U}_\mathbf{v}^\mathbf{T} \mathbf{N} \mathbf{S}_\mathbf{v} \mathbf{d\Gamma}$$

$$\mathbf{A} = \int_{\Gamma_\sigma} \mathbf{U_\Gamma} (\mathbf{N}\mathbf{S}_\mathbf{v})^T d\Gamma$$

$$\mathbf{p_u} = \int_{\Gamma_u} (\mathbf{N}\mathbf{S}_\mathbf{v})^T \bar{\mathbf{u}} d\Gamma$$

$$\mathbf{p}_\sigma = \int_{\Gamma_\sigma} \mathbf{U}_\Gamma^T \bar{\mathbf{t}} d\Gamma$$

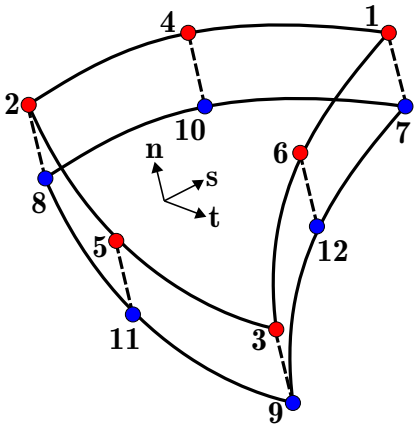

Figure 1: General Interface Element

The size of the problem can be reduced using static condensation. Given that

$$\mathbf{v} = \mathbf{F}^{-1}\mathbf{p_u} + \mathbf{A}^{\mathbf{T}}\mathbf{q} \tag{15}$$

we can obtain a system of equations containing the unknown $\mathbf{q}$ only:

$$(\mathbf{A}\mathbf{F}^{-1}\mathbf{A}^{\mathbf{T}})\mathbf{q} = \mathbf{p}_\sigma - \mathbf{A}\mathbf{F}^{-1}\mathbf{p_u} \tag{16}$$

where $\mathbf{A}\mathbf{F}^{-1}\mathbf{A}^{\mathbf{T}}$ can be considered to be the element stiffness matrix.

3 Interface Elements

Interface elements have traditionally been used to model joints, or interfaces, in rock masses which contained discontinuities, but have been used in modelling fracture of quasi-brittle materials, such as concrete. Interface elements can be used to model fractures with a constitutive relationship relating the tractions and the relative displacement across the interface, following Hillerborg's Fictitious Crack Model [6]. There are two widely used types of interface elements; continuous interface elements and nodal, or point, interface elements [7]. Continuous interface elements, used in this paper, are integrated over the face of the elements on the crack surface while nodal interface elements can be considered to be discrete spring elements. Here, 10-noded tetrahedrons are used for the bulk material and as such 6-noded triangular interface elements are used for the interface element.

Generally, interface elements are inserted into a mesh *a priori* in certain areas of the mesh or along certain paths that cracks are expected to take. This is the approach that was taken in this section of the paper to validate the formulation of the interface element. However, Section 4 will discuss a further implementation of the interface element where they are automatically inserted into a mesh where, and when, they are required.

3.1 Element Formulation

Considering the general interface element in Figure 1, we define a local co-ordinate system where $\mathbf{n}$ is the normal direction to the face and $\mathbf{s}$ and $\mathbf{t}$ are the tangential directions. As such each face has a displacement vector, $\mathbf{q}$

$$\mathbf{q_{face}} = [q_n^1, q_s^1, q_t^1, \ldots, q_n^6, q_s^6, q_t^6]^{\mathbf{T}} \tag{17}$$

and the relative displacement between the faces is given by:

$$\mathbf{g} = \mathbf{q}_{\mathbf{face}}^u - \mathbf{q}_{\mathbf{face}}^l \tag{18}$$

where u and l signify the upper and lower faces on the interface element. This relationship then allows the relative displacement at any point on the element surface to be found using the standard isoparametric shape functions. Transformation of variables to the global co-ordinate system can be obtained using a rotation matrix, $\mathbf{R}$:

$$\mathbf{R} = \begin{bmatrix} n_1 & n_2 & n_3 \\ s_1 & s_2 & s_3 \\ t_1 & t_2 & t_3 \end{bmatrix} \tag{19}$$

where n_i are the components of the normal vector to the face and s_i and t_i are components of the tangential vectors to the face. To obtain the interface stiffness matrix, $\mathbf{K_{int}}$, we consider the principal of virtual work in the standard form [8]. The internal work of the interface element is given by:

$$U = \frac{1}{2} \int_{\Gamma_{int}} \mathbf{U_\Gamma g}.\mathbf{R^T t_{loc}}\, d\Gamma \tag{20}$$

where $\mathbf{t_{loc}}$ is the vector containing the tractions normal and tangential to the face of the element and is related to the local relative displacement across the interface via the interface moduli matrix, $\mathbf{D}$:

$$\mathbf{t_{loc}} = \mathbf{D(g)g} \tag{21}$$

Given that the relative displacement, $\mathbf{g}$, can be approximated over the face of the element by $\mathbf{U_\Gamma}$ then the virtual internal work of the interface element can be written as:

$$U = \frac{1}{2}\mathbf{u_v^T} \int_{\Gamma_{int}} \mathbf{U_\Gamma^T R^T D R U_\Gamma} d\Gamma \mathbf{u_v} \tag{22}$$

where $\mathbf{u_v}$ is a virtual relative displacement in the global co-ordinate system. The virtual external work for the interface element can be described by:

$$W = -\mathbf{u_v^T f} \tag{23}$$

where $\mathbf{f}$ is the external force vector. Thus, the stiffness matrix, $\mathbf{K_{int}}$, and internal force vector are:

$$\mathbf{K_{int}} = \int_{\Gamma} \mathbf{U}_\Gamma^T \mathbf{R}^T \mathbf{D R U_\Gamma} d\Gamma \tag{24}$$

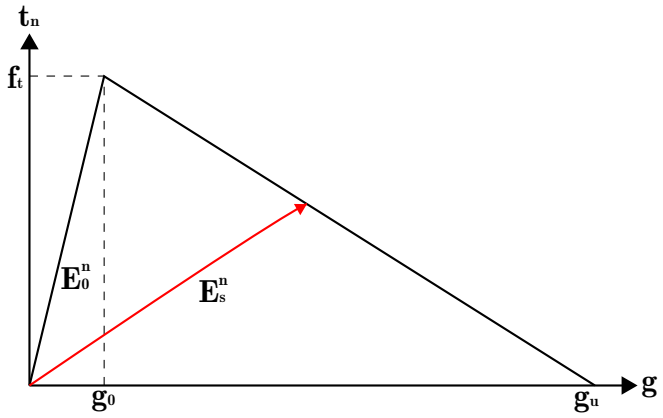

Figure 2: Constitutive Law of Cohesive Crack

$$\mathbf{f_{int}} = \int_{\Gamma} \mathbf{U}_{\Gamma}^{T} \mathbf{R}^{T} \mathbf{t}_{loc} d\Gamma \tag{25}$$

3.2 Cohesive Crack Model for the Interface Element

To test the effectiveness of the formulation outlined above, a relatively simple linear softening law was adopted for the cohesive crack model of the interface element. This softening law is illustrated in Figure 2.

The normal traction across the interface is related to the relative displacement in the normal direction. Separate softening laws can be implemented for the tangential directions but here it was assumed that the stiffness was infinite (E_{∞}) and as such no relative displacement could take place. Therefore the matrix, $\mathbf{D}$, containing the constitutive relationship is:

$$\mathbf{D} = \begin{bmatrix} E_s^n & 0 & 0 \\ 0 & E\infty & 0 \\ 0 & 0 & E\infty \end{bmatrix} \tag{26}$$

While the automatic insertion of cracks when, and where, required was the ultimate goal, an initial analysis was carried out when interface elements were *a priori* present in a mesh. A penalty stiffness was employed to ensure that the analysis behaved as expected during the linear-elastic phase. The selection of this penalty stiffness was vitally important. If the value was too low then the linear-elastic solution would diverge from the actual solution, but if it was too high then the system of equations being solved could become ill-conditioned, introducing significant errors and numerical instability. Therefore, a compromise had to be found which largely eliminated both situations.

Softening will occur once the normal traction exceeds the tensile strength, f_t. Then the softening relationship between the normal traction and associated relative displacement (g_0) is introduced, defined by the fracture energy release rate, G_f.

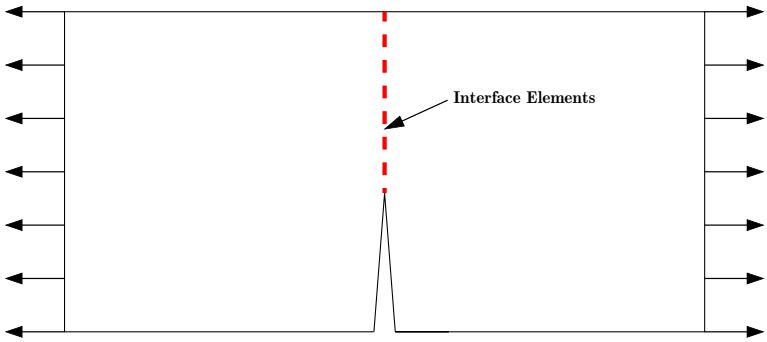

Figure 3: Simple 3D Example

In this work a solution algorithm that utilizes the secant stiffness was adopted. The reason for this is to avoid numerical instabilities sometimes observed when using the tangent stiffness, albeit adopting of the secant stiffness leads to slower convergence. The secant modulus used for the normal component of the softening law is as follows:

$$\begin{cases} E_s^n = E_0^n & \text{when } g \leq g_0 \\ E_s^n = \frac{1}{g}\left[f_t - \frac{f_t^2}{2G_f}\left(g - \frac{f_t}{E_0^n}\right)\right] & \text{when } g_0 < g \leq g_u \\ E_s^n = 0 & \text{when } g > g_u \end{cases} \tag{27}$$

where g is the relative displacement across the interface, g_0 is the relative displacement associated with the onset of softening and g_u is the relative displacement at which the crack is considered to be fully open and can no longer transfer any tractions across it.

A history parameter was also introduced to record the largest relative displacement across the interface element, to ensure that the irreversible behaviour was captured. The penalty stiffness was also used to enforce zero overlap at any cracks that were opened and then subsequently closed.

3.3 Numerical Test of Interface Element

To test the effectiveness of the interface elements use in conjunction with the hybrid-Trefftz stress elements a simple 3D numerical test was carried out, shown in Figure 3. Here, a specimen with a predefined notch is loaded in tension.

Interface elements were inserted *a priori* in the vertical plane directly above the notch in the specimen. A prescribed displacement was applied at either end of the specimen, as indicated, to allow the cracking to occur in the normal direction to the interface element's orientation. PETSc [9] was used to solve the non-linear system of equations using a Newton-like solver. The Load vs Displacement Response for the bottom right hand corner in Figure 4. The expected non-linear response was captured and the solution was obtained without numerical instabilities.

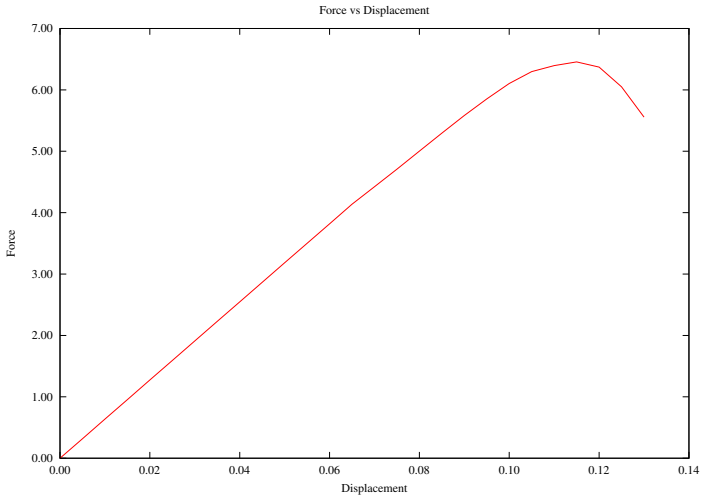

Figure 4: Load vs Displacement Response

4 Crack Insertion Algorithm

Traditionally, interface elements are inserted either between every face of the mesh [10] or in areas where is it believed that fracture will occur. However, there are several issues associated with this approach that need to be considered. Firstly, the number of degrees of freedom will increase dramatically and Needleman [10] suggested that an increase in the computational time of an analysis by roughly 2 compared to a conventional finite element formulation could be observed. Secondly, errors can be introduced to the linear-elastic result, as the penalty stiffness must be employed to ensure that the results are admissible. Therefore, if a very large number of interface elements are employed *a priori* in a mesh, the solutions obtained could be inaccurate.

To remove these disadvantages, an algorithm is presented which allows interface elements to be inserted when required, thereby avoiding problems associated with large scale use of interface elements from the beginning of an analysis. The algorithm presented can be used for inserting of 6-noded triangular interface elements.

4.1 Face Splitting Methodology

The methodology for crack insertion presented is based on the work of Pandolfi and Ortiz [3] but does not use the data structure proposed in their paper. The work carried out here uses the Mesh-Oriented datABase (MOAB) [11] for "book keeping" of mesh data to allow efficient storage.

The selection of faces to be split is based on two conditions. Firstly, the normal traction across a face between two 10-noded tetrahedrons must exceed the tensile strength, f_t, of the material and this is checked at every Gauss point on the face of the element. Secondly, cracks can only initiate if at least one edge of the face, where the tensile strength is exceeded, is on the edge of the domain of the problem. If both

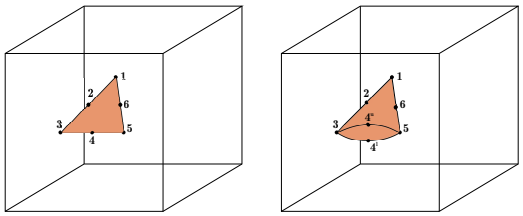

(a) One Element Edge on Surface

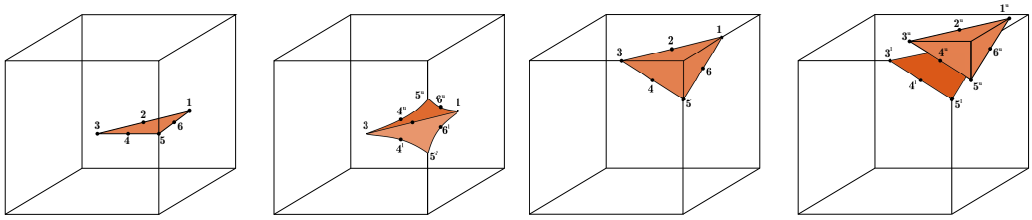

(b) Two Element Edges on Surface (c) Three Edges on Surface

Figure 5: Node Splitting Procedure, based on [3]

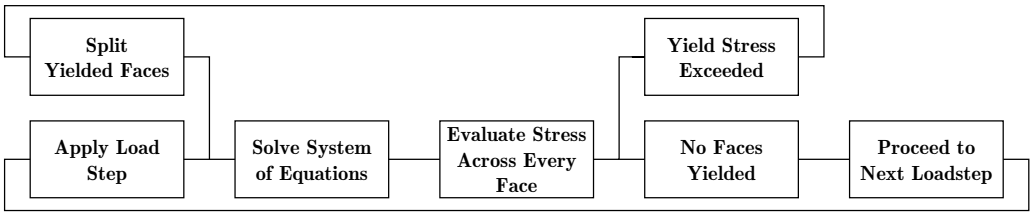

Figure 6: Load Step Procedure

of these conditions are met then the face is marked for splitting and a new face is created in the data structure. Once a new face has been created there are three different options that can be implemented.

- Option (a): If one edge of the face is on the mesh surface then the mid-side node of this edge is split and a new node is added to the mesh.
- Option (b): If two edges of the face are on the mesh surface then both mid-side nodes will be split and the node that is on both edges will also be split.
- Option (c): If three edges of the face are on the mesh surface then every node on the face will be split.

These options are demonstrated in Figure 5.

4.2 Numerical Methodology

The interface element insertion procedure for an entire load step can be seen in Figure 6. The load step is applied and the system of equations is solved. If the normal

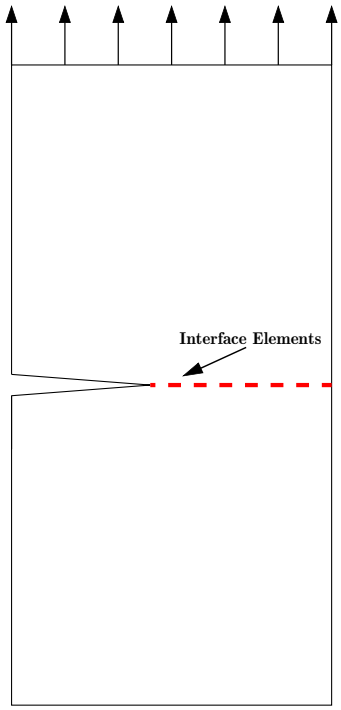

Figure 7: 3D Problem for Crack Insertion

tractions exceed the tensile strength, an interface element is inserted and the load step is repeated. Initially, the penalty stiffness is used to ensure that, when re-running the load step, the elastic response is reproduced. When a crack occurs there is a re-distribution of stresses in the surrounding material which can cause elastic unloading in the surrounding areas. Therefore, the initial inclusion of the penalty stiffness will permit this stress re-distribution to occur as expected, without spurious softening in new interface elements that should behave elastically.

4.3 Numerical Example

A simple 3D problem, shown in Figure 7, was used to investigate the effectiveness of the crack algorithm proposed. Once again, a predefined notch has been inserted into a prismatic specimen subject to tension. A prescribed displacement was applied to one end of the specimen, while the other end was fixed in the vertical direction. The interface elements were limited to insertion on a single plane, indicated by the red line, although they were not present *a priori* as before. The results for the crack insertion and crack separation can be seen in Figure 8. From these results is can be seen that the crack insertion algorithm is working as intended and is allowing crack propagation to occur in a stable manner. Figure 8c has had its displacements exaggerated to allow the crack opening to be visualised. The result presented indicate that the interface elements are behaving in an appropriate manner after insertion.

In future, a softening law will be implemented which allows relative displacement

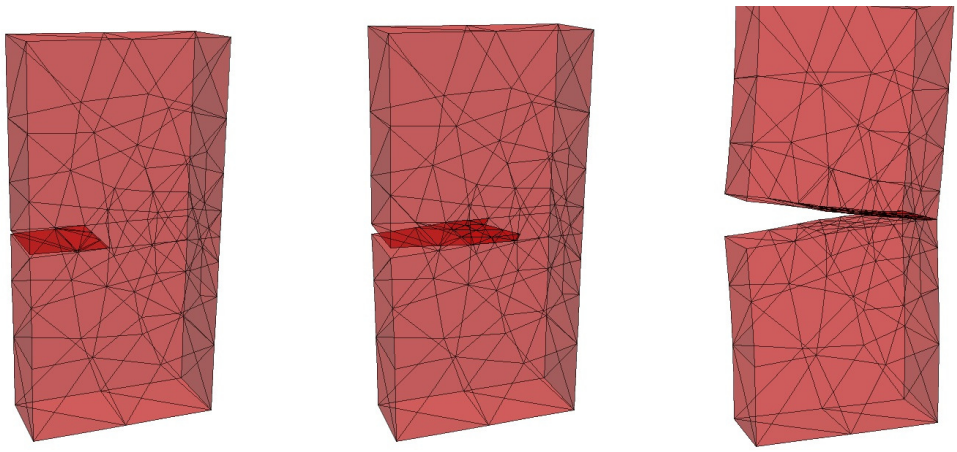

(a) Start of Analysis (b) Insertion of Interface Elements (c) Final Load Step

Figure 8: Results for Crack Insertion Algorithm

in the tangential direction to be captured and a more sophisticated softening law will be used to more accurately represent the softening behaviour of concrete. Large scale problems will also be investigated, where cracking is not restricted to a predefined plane, and as such the C++ code will be produced to take advantage of parallel processing.

5 Conclusion

A formulation for the modelling of cracking in quasi-brittle materials has been presented. The formulation comprises hybrid-Trefftz stress elements for the bulk material, combined with interface elements for the inclusion of discrete cracks.

For the interface elements, a continuous element was used over the nodal version. The interface elements presented contained a simple linear softening law defined by the fracture energy to capture cohesive softening of the material. A 3D example was then used to validate the interface element. For this example interface elements were inserted into the mesh *a priori* and a penalty stiffness was used to ensure satisfactory linear elastic behaviour before softening occurred. The relative displacements across the interface element were restricted to occur in the normal direction to the crack face by using an infinite stiffness in the tangential direction. The results presented indicate that the crack propagated as expected and the correct non-linear response was captured.

Finally, this paper presented an automatic crack insertion algorithm which inserted interface elements when required. The procedure was used to increase the computational efficiency of the code and to ensure that some of the issues of implementing

interface elements *a priori* were removed. An example was presented showing the crack algorithm was behaving as intended when the crack insertion was limited to a specific plane in the mesh.

Acknowledgements

The support of the Engineering and Physical Sciences Research Council (EPSRC) through grants 2008 DTA EP/P50418X/1 and 2009 DTA EP/P504937/1 is gratefully acknowledged and appreciated.

References

[1] Ł. Kaczmarczyk and C. J. Pearce. "A corotational hybrid-Trefftz stress formulation for modelling cohesive cracks". Computer Methods in Applied Mechanics and Engineering, 198 (15-16) : 1298–1310, 2009.

[2] R. de Borst. "Some recent developments in computational modelling of concrete fracture". International Journal of Fracture, 86 : 5-36, 1997.

[3] A. Pandolfi and M. Ortiz. "An Efficient Adaptive Procedure for Three-Dimensional Fragmentation Simulations". Engineering with Computers, 18 : 148-159, 2002.

[4] J. A. Teixeira de Freitas, J. P. Moitinho de Almeida and E. M. B. Ribeiro Pereira. "Non-conventional formulations for the finite element method". Computation Mechanics, 23 (5-6) : 488-501, 1999.

[5] J. A. Teixeira de Freitas. "Formulation of elastostatic hybrid-Trefftz stress elements". Computer Methods in Applied Mechanics and Engineering, 153 (1-2) : 127-151, 1998.

[6] A. Hillerborg, M. Modeer and P. Petersson. "Analysis of crack formation and crack growth in concrete by means of fracture mechanics and finite elements". Cement and Concrete Research, 6 (6) : 773-781, 1976.

[7] J. C. J. Schellekens and R. De Borst. "On the Numerical Integration of Interface Elements". International Journal for Numerical Methods in Engineering, 36 : 43-66, 1993.

[8] O. C. Zienkiewicz, R. L. Taylor & J. Z. Zhu. "The Finite Element Method: Its Basis & Fundamentals". Elsevier Butterworth-Heinemann, Oxford, UK, 2005.

[9] S. Balay, J. Brown, K. Buschelman *et. al.* "PETSc Web Page". http://www.mcs.anl.gov/petsc , 22 March 2012.

[10] X. Xu and A. Needleman. "Numerical simulations of fast crack growth in brittle solids". Journal of the Mechanics and Physics of Solids, 42 (9) : 1397-1434, 1994.

[11] T. J. Tautges, J. A. Kraftcheck, B. M. Smith and H-J. Kim. "Mesh Oriented datABase (MOAB) Version 4.0 : User Guide". http://www.mcs.anl.gov/~tautges/MOABv4-UG.pdf, 22 March 2012.